Acta Oceanol. Sin., 2021, Vol. 40, No. 4, P. 10–22
https://doi.org/10.1007/s13131-021-1723-4
http://www.hyxb.org.cn
E-mail: ocean2@hyxb.org.cn

Statistical characteristics and thermohaline properties of mesoscale eddies in the Bay of Bengal

Wei Cui[1], Chaojie Zhou[2]*, Jie Zhang[1], Jungang Yang[1]

[1] First Institute of Oceanography, Ministry of Natural Resources, Qingdao 266061, China

[2] Hainan Insititute of Zhejiang University, Sanya 572000, China

Received 8 May 2020; accepted 22 June 2020

Abstract

The statistical characteristics and vertical thermohaline properties of mesoscale eddies in the Bay of Bengal are studied from the view of satellite altimetry data and Argo profiles. Eddy propagation preferences in different lifetimes, eddy evolution process, and geographical distribution of eddy kinetic properties are analyzed in this area. Eddies exist principally in the western Bay of Bengal, and most of them propagate westward. There is a clear southward (equatorward) preference for eddies with long lifetimes, especially for cyclones. Moreover, the eddies in different areas of the bay show different north-southward preferences. Evolution of eddy kinetic properties with lifetime shows that eddies have the significant three-stage feature: the growth period in the former one-fifth lifetime, the stable period in the middle two-fifth to four-fifth lifetime, and the dying period in the last one-fifth lifetime. Large-amplitude and high-intensity eddies occur only in the relatively confined regions of highly unstable currents, such as the East Indian Coastal Current and eastern Sri Lanka. Based on Argo profile data and climatology data, the eddy synthesis method was used to construct three-dimensional temperature and salt structures of eddies in this area. The mean temperature anomaly is negative/positive to the cyclonic/anticyclonic eddies in the upper 300×10^4 Pa, and below this depth, the anomaly becomes weak. The salinity structures of positive anomalies inside cyclonic eddies and negative anomalies inside anticyclonic eddies in the Bay of Bengal are not consistent with other regions. Due to the special characteristics of the water mass in the bay, especially under the control of the low-salinity Bay of Bengal water at the surface and the Indian equatorial water in the deep ocean, the salinity of seawater shows a monotonic increase with depth. For regional varieties of temperature and salinity structures, as the eddies move westward, the temperature anomaly induced by the eddies increases, the effecting depth of the eddies deepens, and the salinity structures are more affected by inflows. In the north-south direction, the salinity structures of the eddies are associated with the local water masses, which comprise low-salinity water in the northern bay due to the inflow of freshwater from rivers and salty water in the southern bay due to the invasion of Arabian Sea high-salinity water from the north Indian Ocean.

Key words: mesoscale eddy, Bay of Bengal, thermohaline structures, satellite altimetry, Argo data

Citation: Cui Wei, Zhou Chaojie, Zhang Jie, Yang Jungang. 2021. Statistical characteristics and thermohaline properties of mesoscale eddies in the Bay of Bengal. Acta Oceanologica Sinica, 40(4): 10–22, doi: 10.1007/s13131-021-1723-4

1 Introduction

Oceanic vortices are ubiquitous in the ocean, and their dynamics are key components in the evolution of water column properties. Mesoscale eddies are rotating coherent structures of ocean currents, which generally refer to ocean signals with spatial scales from tens to hundreds of kilometers and time scales from days to months (Robinson, 2010). Combination altimetry data (since the launch of the TOPEX/Poseidon in 1992) with other satellite missions, *in situ* measurement data and an ocean model is used frequently in modern ocean research (Le Traon et al., 2003; Pascual et al., 2006; Lou et al., 2011), and has provided a significant contribution for mesoscale eddy observations (Cui et al., 2019; Le Traon and Dibarboure, 2004; Thompson et al., 2014). Over recent decades, mesoscale eddies have been found to exist nearly everywhere in the world's oceans (Chelton et al., 2011b; Xu et al., 2011; Fu, 2009), and they impact biological activities, tracer transport, and water column properties (Chelton et al., 2011a; Dong et al., 2014; Zhang et al., 2014). By combining satellite altimetry and Argo profiling float data, the analysis of eddy three-dimensional structure becomes an important part of studying the oceanic eddy (Chaigneau et al., 2011; Liu et al., 2012; Yang et al., 2013; Amores et al., 2017).

The Bay of Bengal, the largest bay in the world, forms the northeastern part of the Indian Ocean. As these bathymetric constraints, the local ocean dynamics is complex, with a broad spectrum of processes, from a seasonal reversing monsoon, cyclonic storms, small-scale river plumes, instabilities generated near the continental slope, eddies and large-scale circulation (Eigenheer and Quadfasel, 2000; Vinayachandran et al., 1999). Overall, the southwest monsoon prevails over the Bay of Bengal in summer, and alternate cyclonic and anticyclonic circulation cells prevailed in the western bay; cyclone-like circulation at the basin-

Foundation item: The National Key Research and Development Program of China under contract No. 2016YFC1401800; the Basic Scientific Fund for National Public Research Institutes of China under contract No. 2020Q07; the National Natural Science Foundation of China under contract No. 41576176; the Dragon 4 Project under contract No. 32292; the National Programme on Global Change and Air-Sea Interaction under contract Nos GASI-02-PAC-YGST2-04, GASI-02-IND-YGST2-04 and GASI-02-SCS-YGST2-04.
*Corresponding author, E-mail: hitzcj@163.com

scale during the fall monsoon transition; whereas a stronger northeast monsoon dominates the bay in winter, and the upper layer circulation presents large anticyclonic flow during winter; and then the intense winter cyclonic gyre was embedded as cyclonic eddy between two anticyclonic cells in the following spring (Somayajulu et al., 2003; Hacker et al., 1998; Chen et al., 2012). Legeckis (1987) established the possibility of a western boundary current (the East Indian Coastal Current, EICC) in the Bay of Bengal. The EICC reverses direction twice a year, flowing northeastward from February until September and southwestward from October to January (Schott and McCreary, 2001). Affected by complex exogenous effects such as the local monsoon, equatorial remote forcing, and seasonal changes in river runoff, the circulation of the Bay of Bengal has obvious seasonal variation; and studies show that there are abundant mesoscale eddy accompanying these seasonally changing circulations in the Bay of Bengal (Babu et al., 1991; Sarma et al., 1999; Chen et al., 2012; Cheng et al., 2013; Cui et al., 2016).

Many studies on the Bay of Bengal have shown that most eddies exist around EICC (Babu et al., 2003; Cui et al., 2016; Chen et al., 2012, 2018; Cheng et al., 2018). As noted by Somayajulu et al. (2003), the monsoon conversion, EICC instability and energy transmission of westward Rossby waves are the main reasons for the high occurrence of eddies around the western Bay of Bengal. Chen et al. (2012) analyzed the genesis, propagation, mean properties and the spatiotemporal variability of eddies in the bay, and found that the interannual variability of the mesoscale eddies is sensitive to the baroclinic instability of the background flow. Chen et al. (2018) suggested that a complicated mechanism involving both local and remote wind forcing and ocean internal instability is responsible for the generation and modulation of eddy kinetic energy in this region. Cheng et al. (2013) found that eddy activities contribute considerably to the strong sea surface height intraseasonal variability in the central bay and that the high total eddy energy in the western bay is due to the barotropic/baroclinic instability of the mean current.

The three-dimensional structures and heat-salt transport characteristics of mesoscale eddies in the Bay of Bengal can be investigated by the combined use of satellite altimetry and Argo floats. Dandapat and Chakraborty (2016) presented three-dimensional properties of the mesoscale eddies in the western Bay of Bengal and found the cyclonic eddies are generally intensified in the subsurface depths in the western bay. Lin et al. (2019) showed that eddy-induced ocean anomalies are mainly confined to the upper 300 m depth and eddy thermohaline structure has a seasonal character. Gulakaram et al. (2020) quantified the three-dimensional eddy structures in the Bay of Bengal, and the surface eddy centric composite analysis reveals the existence of warm (cold) and diverse SSS anomalies for anticyclonic (cyclonic) eddies. Based on vertical thermohaline data provided by Argo, Gonaduwage et al. (2019) investigated the meridional and zonal eddy-induced heat and salt transport in the Bay of Bengal and their seasonal modulation, and they found that the local wind-stress curl and remote forcing from the equator partly influences the thermocline motion.

Although there have been many analyses of eddies on the surface and some studies of the three-dimensional eddy properties in the Bay of Bengal, the eddy propagation preferences in different lifetimes, eddy evolution process, and geographical distribution of eddy kinetic properties are not well analyzed; in addition, the causes of three-dimensional thermohaline properties of eddies and their regional varieties have not been studied. In this paper, we analyze the statistical characteristics of mesoscale eddies in the Bay of Bengal based on merged satellite altimetry data as well as Argo profile data. First, based on satellite altimeter data, the automatic identification method was used to extract the position and shape information of the mesoscale vortices. Then, a series of statistical analysis methods were used to study the statistical characteristics of the mesoscale eddies in the area, e.g., eddy trajectories and propagation directions, evolution of eddy kinetic properties, and geographical distribution of eddy kinetic properties. Finally, based on Argo profile data and climatology data, the eddy synthesis method was used to construct the three-dimensional temperature and salt structures of eddies in this area, and the thermohaline properties of eddies and their regional varieties were analyzed.

The rest of the paper is organized as follows: Section 2 describes the altimetry and Argo data, as well as the eddy detection methodology. Section 3 presents the census statistics of mesoscale eddy characteristics, including eddy trajectories and propagation directions, evolution of eddy kinetic properties, and geographical distribution of eddy kinetic properties. Section 4 analyzes the three-dimensional temperature and salt structures of eddies and their regional varieties in this area. Finally, the summary and conclusions are given in Section 5.

2 Data and methods

2.1 *Satellite altimeter data and Argo profiles*

The presence and positions of mesoscale eddies were determined by analyzing sea level anomaly (SLA) fields, merged and gridded multimission altimeter products (SEALEVEL_GLO_PHY_L4_REP_OBSERVATION_008_47), which are distributed by the European Copernicus Marine Environment Monitoring Service (CMEMS, marine.copernicus.eu). The daily SLA fields with a spatial resolution of 0.25° spanned a 24-year period from January 1993 through February 2017.

The vertical structures and the effect of eddies on the subsurface temperature and salinity were studied using available Argo profiles in the Bay of Bengal, provided by the Coriolis Global Data Acquisition Center of France through the website http://www.coriolis.eu.org. In our analysis, we have taken pressure, temperature, and salinity profiles with quality flag 1, and have followed Chaigneau et al. (2011) for the selection of the profiles from 2001 to 2017. The final dataset include total 17 945 available profiles in our study region. Potential temperature θ and salinity S data in each profile were linearly interpolated onto 101 vertical levels from the surface to $1\,000\times10^4$ Pa with an interval of 10×10^4 Pa using the Akima spline method.

To get the thermohaline structures of mesoscale eddies, potential temperature anomaly θ', and salinity anomaly S' of Argo profiles were computed by removing climatologic profiles. In our study, the climatologic θ/S profiles were obtained by interpolating the 0.5°×0.5° standard-level climatologic fields of CSIRO Atlas of Regional Seas 2009 (CARS 2009) linearly onto 0.1°×0.1° fields to get a more accurate match with the Argo profile locations.

2.2 *SLA-based eddy identification and tracking*

Oceanic mesoscale eddies can generally be identified as regions enclosed by SLA contours within which water slugs of unique characteristics are trapped and subsequently translated. A purely geometric algorithm for eddy identification based on the outermost closed contour of an SLA has been proposed by Chelton et al. (2011b). After the identification, we computed an estimate of different eddy characteristics. The amplitude AM of an eddy is defined as the absolute value of the SLA difference

between the eddy center and its edge. The eddy size is represented by the eddy area A, which is delimited by the outermost-closed eddy boundary. The eddy scale/radius R corresponds to the equivalent radius of a circle that has the same area as the region within the eddy perimeter. The eddy intensity or eddy energy can be quantified through the eddy kinetic energy (EKE) over the eddy area, $\mathrm{EKE} = \frac{1}{2}(u'^2 + v'^2)$ and u' and v' are the zonal and meridional geostrophic velocity components, respectively. The maximum rotational speed $U_{\max}$ of an eddy corresponds to the speed of that enclosed by the contour with maximum circum-average geostrophic velocity.

The eddy trajectory can be tracked by comparing the centers and other characteristics in the continuous time series of the SLA fields (Chaigneau et al., 2008; Henson and Thomas, 2008; Nencioli et al., 2010; Souza et al., 2011). In the tracking procedure, the trajectory of a given eddy at the time step n is identified by searching the most similar eddy at the subsequent time step n+1 in terms of the type (cyclonic/anticyclonic) and eddy characteristics in a restricted region around the eddy center at the time step n (Chaigneau et al., 2008; Chen et al., 2012). The lifetime of an eddy represents the duration of an eddy from its generation to its termination, and the propagation distance of an eddy is represented by the relative spatial displacement of the eddy throughout its lifetime.

2.3 *Composite eddy reconstruction*

In order to study the three-dimensional thermohaline properties of mesoscale eddies in the Bay of Bengal, it is important to relate Argo θ/S data with the eddy signals at the sea surface detected by AVISO altimeters. In this study, all the eddies with lifetime no less than 30 d are used for eddy composition. Following Chaigneau et al. (2011), three-dimensional structures of eddies were constructed by surfacing the Argo float profiles into SLA-based eddy areas. For each eddy, we searched the Argo float profiles located in its edge and calculated the relative ΔX and ΔY corresponding to the eddy center at ΔX=ΔY=0 for each Argo float profile. We matched the cyclonic and anticyclonic eddies observed by the satellite altimeter with the corresponding Argo profiles for the same day and selected the Argo profiles within eddies or outside eddies but not beyond 1.5 times the eddy radius for composite eddy reconstruction. Thus, the 17 945 Argo profiles are classified into three categories: a total of 2 389 Argo profiles are used for anticyclonic eddy reconstruction, of which 1 142 are inside cyclones; a total of 2 346 Argo profiles are used for anticyclonic eddy reconstruction, of which 1 249 are inside anticyclones; and 13 210 are outside eddies in this region.

For each Argo profile matched by an eddy, we calculated the normalized position (Δx, Δy) relative to the eddy radius, which is calculated by (ΔX, ΔY) divided by the eddy radius R. For the Argo profiles, θ', S' profiles are computed by removing daily mean climatologic profiles of CARS 2009. Then, all θ, S and θ', S' data are transformed into normalized eddy-coordinate space (Δx, Δy) and mapped onto 0.1×0.1 grids by inversed distance weighting interpolation.

3 Statistical eddy characteristics

A statistical analysis of the eddies detected by the automated tracking procedure from January 1993 to February 2017 in the Bay of Bengal is presented in this section. As a result, 1 089 eddies, which include 583 cyclones (36 065 independent eddy) and 506 anticyclones (29 547 independent eddy), with lifetimes ⩾30 d are detected in the eddy tracking procedure, and a regional census statistic is performed on 1 089 eddies.

3.1 *Eddy trajectories and propagation directions*

The propagation directions and movement characteristics of eddies in the Bay of Bengal can be displayed by analyzing the eddy trajectories. Most mesoscale eddies (approximately 90% cyclones and 93% anticyclones) propagate westward in the Bay of Bengal, which consistent with previous studies (Chen et al., 2012; Cui et al., 2016; Lin et al., 2019). Conversely, less eddies have net eastward displacement, and they have much smaller lifetimes and much shorter propagation distances than the westward eddies. These eastward eddies mostly propagate eastward with the action of some strong currents and the effects of strong monsoons, especially the eddies restricted to near EICC can be expected from advection of the eddies by the seasonal northeast currents (Cui et al., 2016; Kumar and Chakraborty, 2011). Short-lived eastward eddies are closely associated with strong current variations and complicated dynamic processes because of air-sea interactions (Chen et al., 2012).

The analysis of these trajectories with lifetimes⩾30 d in the Bay of Bengal shows that 53% cyclones and 55% anticyclones propagate southward (equatorward), with eddy lifetime increasing to 60 d, 90 d, 120 d, the ratios turn into 63% and 60%, 69% and 64%, 78% and 70% (Table 1), respectively. With the increasing lifetime, the difference in the number of northward eddies and southward eddies becomes more and more obvious: for eddies with lifetimes⩾90 d, the number of southward eddies is double the number of northward eddies (67%:33%); for eddies with lifetimes⩾120 d, the number of south-north eddies differs by three times (75%:25%). The result reveals that there is a clear southward (equatorward) preference for eddies with long lifetimes in the Bay of Bengal, especially cyclones.

The eddies in different areas of the Bay of Bengal show different north-southward preferences (Fig. 1). In terms of the northward and southward eddies with lifetimes⩾60 d, the northward eddies are mainly distributed in the southern bay, while the southward eddies are mainly located in the middle and northern bay. It can be clearly seen that at the dividing line of 12°N, the eddies to the south of the line mostly propagate northwestward, and the eddies to the north of the line mostly propagate southwestward. The meridional eddy movement pattern was like that found in Chen et al. (2012) and Lin et al. (2019). Most of the northward eddies originate mainly outside the bay and in the southern bay (south of 12°N), and then propagate into the western bay along the southwest monsoon current; there are also some eddies formed in the southwestern bay that will enter the western bay from advection of the northward EICC (Fig. 1a). The eddies generated in the northern and middle bay (north of 12°N)

Table 1. The number of southward and northward eddies with different lifetimes, and their proportion (southward/northward)

	Lifetime⩾30 d	Lifetime⩾60 d	Lifetime⩾90 d	Lifetime⩾120 d
Southward	**586** (CE: 307; AE: 279)	**281**(CE: 147; AE: 134)	**136**(CE: 78; AE: 58)	**77** (CE: 46; AE: 31)
Northward	**503**(CE: 276; AE: 227)	**176** (CE: 88; AE: 88)	**68** (CE: 35; AE: 33)	**26**(CE: 13; AE: 13)
Proportion	**54:46**(CE: 53:47; AE: 55:45)	**61:39** (CE: 63:37; AE: 60:40)	**67:33** (CE: 69:31; AE: 64:36)	**75:25** (CE: 78:22; AE: 70:30)

Note: Bold numbers represent all eddies; CE and AE mean cyclonic and anticyclonic eddies, respectively.

mostly propagate southwest due to topographical constraints, and in the southern bay, few eddies propagate south to the area outside the bay (Fig. 1b). Cheng et al. (2018) suggested that when equatorial wind-driven downwelling (upwelling) Kelvin waves propagate to the tip of the Irrawaddy Delta off Myanmar, eddies in the central bay are generated there with periods of 30–120 d that subsequently propagate southwestward. The eddies with different propagation preferences in the northern and southern bay are very important for water transport in the Bay of Bengal. For example, eddies to the south of 12°N mostly propagate northward and disappear in the background field in the western bay, and they will transport the Arabian Sea High-Salinity Water (ASHSW, Fig. 4) near the equator into the western Bay of Bengal. These high-temperature and high-salt waters will continue to be transported to the northern bay along with the northward EICC and even affect the temperature and salt structure in the whole bay. In contrast, eddies to the north of 12°N mostly propagate southward and will carry low-temperature, low-salt, and low-density waters from river runoff and net precipitation to the middle and southern bay, which will affect the temperature and salinity and circulation structure of the entire Bay of Bengal.

3.2 *Evolution of eddy kinetic properties*

The averaged kinetic properties of eddies in different lifetimes show that the eddies with longer lifetime have the stronger kinetic properties in the Bay of Bengal. That is to say, the stronger eddies can maintain a more stable and uniform rotational structure to ensure that they can last a longer lifetime in the ocean. The changes of eddy kinetic properties during the evolution of eddies with different lifetimes are shown in Figs 2a–c. Eddy properties are generally low in the eddy generation and disappearance stages, and eddy properties are generally high in the middle maturation stage of the eddy lifetime. The kinetic properties of all eddies exhibit symmetrical and parabolic changes with the eddy evolution in the complete lifetime. Moreover, the eddy properties in different lifetimes are basically same in the eddy generation and disappearance stages. On average, no matter eddies with what longer lifetime in the Bay of Bengal, eddies generally have an amplitude of 4 cm, a radius of 75 km, and an EKE of 1×10^4 cm^2/s^2 when they appear or disappear in the ocean. The eddy properties in different lifetimes have the largest difference in the middle maturation stage of the eddy lifetime. The max amplitude of eddies with lifetimes of 30–60 d generally does not exceed 8 cm, while the max amplitude of eddies with lifetimes $\geqslant$ 150 d can reach 16 cm in the middle lifetime stage. Generally speaking, in the stable and mature stage of eddy evolution, the eddies with longer lifetime have the stronger kinetic properties; while in the eddy generation and disappearance stages, the eddies with different lifetimes have the similar kinetic properties.

The relative changes of eddy kinetic properties during the lifetime evolution are shown in Figs 2d–f. From the figure, it can be clearly seen that the eddy properties increase significantly in the former one-fifth stage of the lifetime, in which the eddy amplitude increase by more than 1 times, the EKE increase by more than 4 times, and the eddy radius also increase significantly. The middle 2/5 to 4/5 of lifetime is the stable and mature stage of eddies. At this stage, eddy properties are relatively stable, and the eddy energy density is very concentrated; the eddy amplitude and radius are both at 90% of the maximum value. The last 1/5 stage of the lifetime is the dying period of eddies, which is exactly the opposite of the first 1/5 stage of lifetime. During this period, the eddy kinetic properties decrease rapidly, and finally the eddy disappears in the ocean.

3.3 *Geographical distribution of eddy kinetic properties*

The automated eddy identification provides the estimates of the eddy amplitude, radius scale and EKE as defined in Section 2.2. These kinetic properties of eddies with lifetimes $\geqslant$30 d over a 24-year period are analyzed here. There are some differences between the average properties of cyclones and anticyclones in the Bay of Bengal (Table 2). Specifically, the average amplitude and radius of cyclonic eddies are 9.7 cm and 116 km, and that of

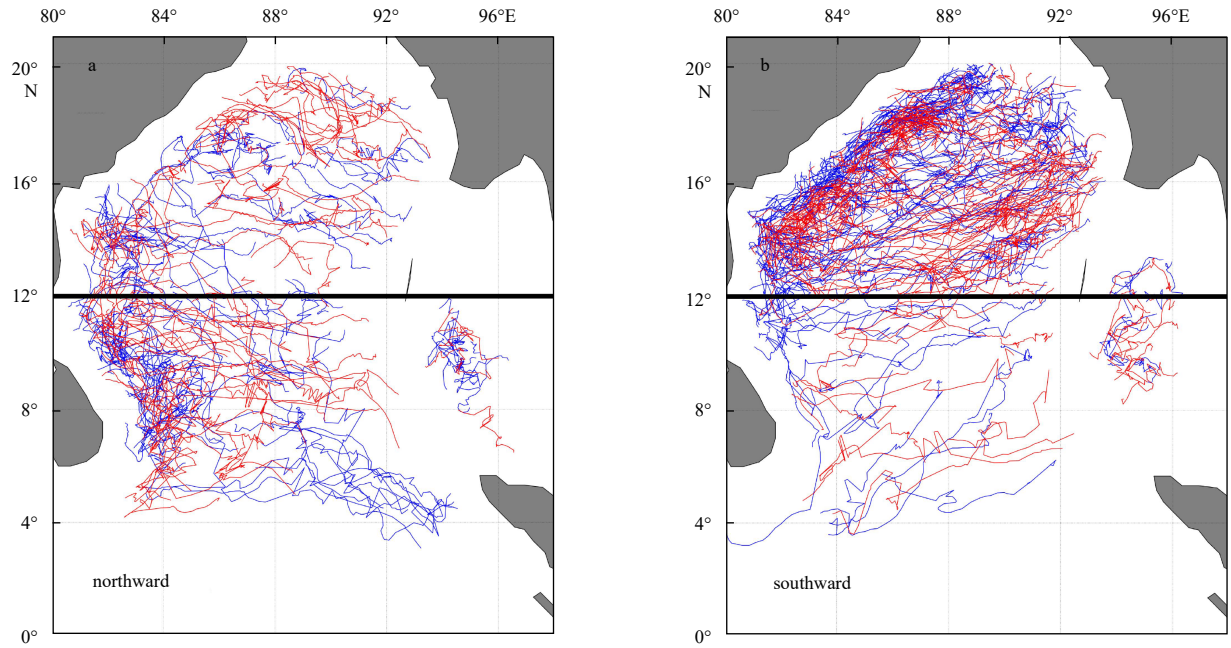

Fig. 1. The northward (a) and southward (b) propagation trajectories of the cyclonic (blue lines) and anticyclonic (red lines) eddies with lifetimes$\geqslant$60 d.

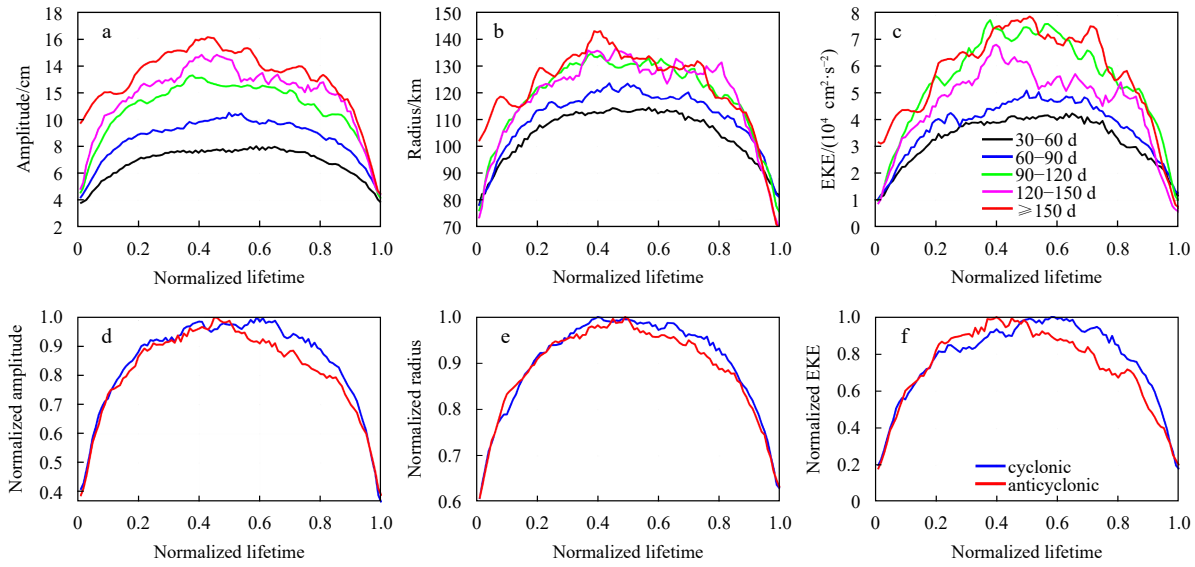

Fig. 2. Evolution of eddy kinetic properties with the lifetime. a–c. The changes of eddy kinetic properties during the evolution of eddies with different lifetimes. The eddies with different lifetimes are divided into five categories: [30, 60) d, [60, 90) d, [90, 120) d, [120, 150) d, and langer than 150 d (the numbers of cyclonic and anticyclonnic eddies are: 348 and 284, 122 and 131, 54 and 47, 20 and 22, 39 and 22, respectively). Here cyclonic and anticyclonic eddies are considered together, and the eddy lifetime has been normalized. d–f. The normalized relative properties of all cyclonic (blue line) and anticyclonic (red line) eddies with lifetime⩾30 d evolve with the normalized lifetime.

Table 2. Average kinetic properties of eddies with lifetimes⩾30 d in the Bay of Bengal

	AM/cm	R/km	EKE/(cm^2·s^{-2})	U_{max}/(cm·s^{-1})
Cyclones	9.70	116	4.70×10^4	41.5
Anticyclones	9.00	122	3.78×10^4	36.4

anticyclonic eddies are 9.0 cm and 122 km. The average amplitude intensity of anticyclonic eddies is smaller than that of cyclones, but the spatial scale is larger than that of cyclones. Although the radius of cyclonic eddies is small, their average eddy kinetic energy EKE (4.7×10^4 cm^2/s^2) is significantly larger than that of anticyclones (3.78×10^4 cm^2/s^2), indicating that the ocean kinetic energy carried by cyclonic eddies is more concentrated (higher eddy energy density). Of course, the magnitude of eddy energy is more intuitively reflected in the rotational speed of eddies. In terms of the maximum rotational speed U_{max}, cyclonic eddies (41.5 cm/s) are significantly larger than anticyclonic eddies (36.4 cm/s), indicating that the cyclonic eddies rotate faster than the anticyclones in the Bay of Bengal. This outcome is likely related to the intrusion of the offshore monsoon current caused by the summer southwest monsoon in the southwestern bay. During this period, many intense cyclonic eddies are generated in the eastern region of Sri Lanka, and the cyclones generally rotate very fast with the intrusion of the monsoon current (Nuncio and Kumar, 2012; Chen et al., 2018). In general, cyclonic eddies are stronger than anticyclones in terms of eddy amplitude, EKE, and maximum rotational speed, but the spatial scale of cyclones is smaller than that of anticyclones, which means that cyclones have a higher eddy energy density than anticyclones.

The numbers of eddy occurrences for cyclonic and anticyclonic eddies are shown in Figs 3a and b. Although the Bay of Bengal region is not large enough for longer lifetime eddies due to the topography constraints, there are also abundant mesoscale eddies in the bay similar to the world's oceans (Chelton et al., 2011b). Especially, eddies are concentrated in the northwestern bay, where the seasonal western boundary current EICC exists. An important reason for the distribution is the baroclinic instability of the EICC induced by a middle topography mutation of the western bay and by the local monsoon conversion (Babu et al., 1991; Hacker et al., 1998; Cui et al., 2016; Chen et al., 2012, 2018). From the polarity geographical distribution (Fig. 3c), it can be seen that the preferences of cyclones or anticyclones are indistinctive (values of P are near 0) in most regions of the Bay of Bengal, e.g., in the northern, central and southern bay where there are similar numbers of cyclones and anticyclones. However, there are still slight preferences in some local regions. Separately, the western bay and the southern region outside the bay tend to the occurrence of cyclonic eddies, while in the eastern bay (specifically, the region of 12°–16°N, 88°–94°E) there is a slight preference for the anticyclonic eddy occurrences. It is worth noting that near the southeastern region outside the bay (the northwest of Sumatra), the eddy polarity P shows significant negative values, indicating that the number of cyclones is significantly greater than that of anticyclones. This outcome occurs because a large number of cyclonic eddies often occur near the eastern region of Sumatra Island (5°N, 93°E), and they gradually move northwest into the Bay of Bengal or disappear into the southern bay mouth (Fig. 1a). Chen et al. (2017) show that in addition to local wind and current instability, parts of eddy energy in the Bay of Bengal originates from the equator. Equatorial-origin wave signals significantly enhance the EKE levels in the northwest of Sumatra, in the form of reflected Rossby waves and coastal Kelvin waves, respectively (Chen et al., 2018).

The maps of the mean amplitude (Figs 3d and e), radius (Figs 3g and h), and EKE (Figs 3j and k) of cyclonic and anticyclonic eddies are shown in Fig. 3, and their variations with latitude are also shown in Figs 3f, i, and l. In terms of eddy amplitude, approximately two thirds of all detected eddies have amplitudes <10 cm, and 15% have amplitudes >15 cm in the Bay of Bengal,

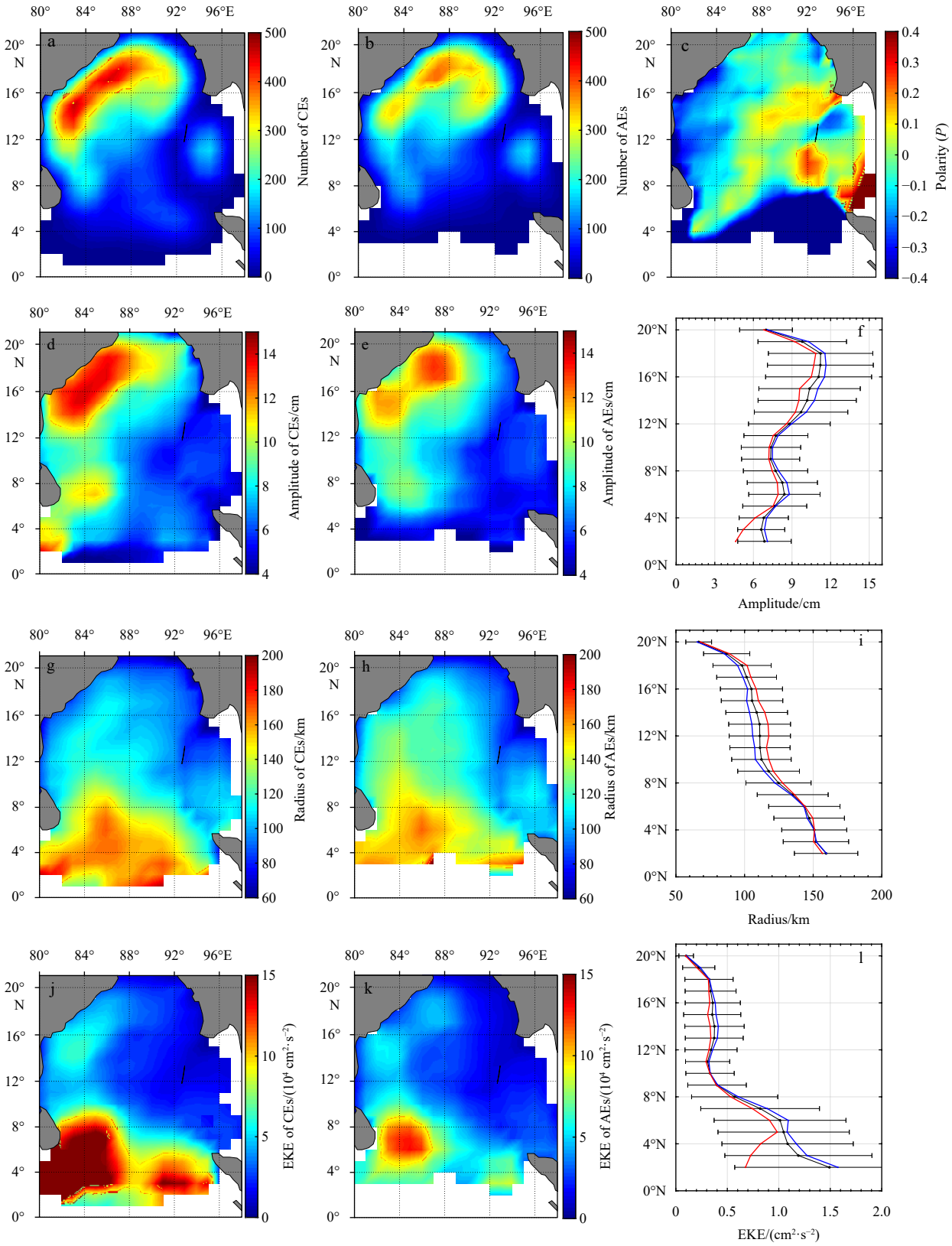

Fig. 3. Census statistics for numbers (a and b) of cyclonic (CEs) and anticyclonic (AEs) eddies and their polarity distribution (c) for each 1°×1° region (smoothed using a 3°×3° window), the maps of the mean amplitude (d and e), radius (g and h), and EKE (j and k) of CEs and AEs, and their variations with latitude (f, i, and l). The red and blue lines in f, i and l represent the mean zonal properties of CEs and AEs, respectively; and the black lines represent the mean zonal properties and standard deviations of all eddies.

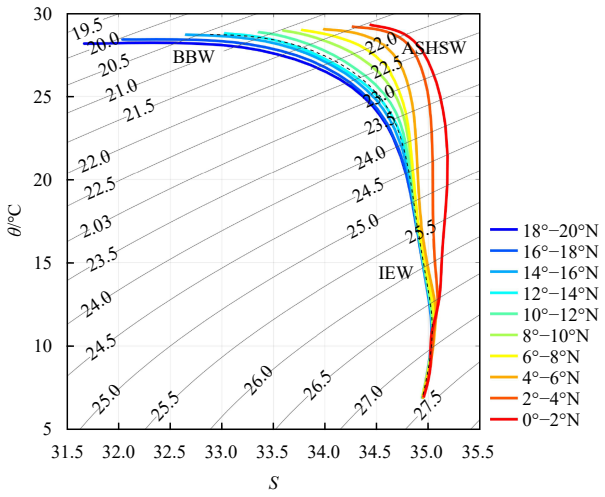

Fig. 4. Mean potential temperature and salinity (θ-S) diagram calculated at different latitudes (color lines) based on all Argo profiles in the Bay of Bengal. Gray contours denote potential density σ (kg/m^3), and the black dotted line is the mean θ-S profile in the whole bay (4°–20°N, 80°–94°E).

which consistent with Cui et al. (2016) and Lin et al. (2019). From the maps of mean eddy amplitude (Figs 3d and e), eddies with large amplitudes occur only in the relatively confined regions of highly unstable currents, such as the EICC and eastern Sri Lanka where eddies have amplitudes>12 cm (especially, near the EICC amplitudes>15 cm); over the rest of the bay, the mean eddy amplitudes are generally less than 10 cm. The large-amplitude eddies most likely form as meanders that pinch off the western boundary currents, or from baroclinic instability in the regions of strong and unstable currents. Chen et al. (2012) suggested that when the baroclinic instability is stronger, more energy from the mean is converted to the eddy energy, which makes eddies stronger and more stable but fewer in number. Moreover, the EICC is a very obvious seasonally changing current, and during the southwest monsoon in summer and the northeast monsoon in winter, the flow direction is completely opposite. Therefore, during the turn of the current, more large-amplitude eddies are more likely to be generated due to the instability of the EICC (Cheng et al., 2013; Chen et al., 2018). In eastern Sri Lanka, due to the intrusion of the southwest monsoon current and the effect of negative wind stress curl, there are often eddy-train structures in which strong cyclones and anticyclones alternately move northwest into the western bay in summer and autumn (Cui et al., 2016; Kumar and Chakraborty, 2011; Vinayachandran et al., 1999). Therefore, the eddy amplitudes are also high in eastern Sri Lanka. Generally, compared with eddy amplitudes in the regions of strong western boundary currents (e.g., the Gulf Stream and Kuroshio extensions; Cui et al., 2017; Fu, 2009; Chelton et al., 2011b), the mean eddy amplitude in the Bay of Bengal is lower, and the number of large-amplitude eddies is fewer. This outcome occurs mainly because the Bay of Bengal has only a seasonal western boundary current EICC that changes with the monsoon, and its velocity and intensity are not as strong as other western boundary currents in the world's oceans (Cheng et al., 2013).

The eddy radii are mainly scattered in 50–150 km for approximately 80% eddies in the Bay of Bengal. This latitudinal dependence of eddy scale is evident from the geographical distributions of the mean radius of cyclonic and anticyclonic eddies (Figs 3g and h), which are characterized as an essentially monotonic increase from approximately 60 km at 20° latitude to approximately 160 km in the near-equatorial regions (Fig. 3i). This latitudinal dependence of eddy scale is closely related to the Rossby radius of deformation (Chen et al., 2012; Lin et al., 2019). The eddy radii in the central of the bay are greater than that in the nearshore area. In terms of eddy polarity, the radii of anticyclonic eddies are larger than those of cyclones at most latitudes, especially in the western and central bay which similar to the result of Lin et al. (2019); while radii of cyclonic and anticyclonic eddies are not much different in the low-latitude regions (Fig. 3i). It shows that the eddy scale difference between the cyclones and anticyclones is limited to the interior of the bay.

The geographical distributions of the mean EKE (Figs 3j and k) are consistent with the eddy scale. Although the mean scale of anticyclonic eddies is larger than that of cyclones, the latter carries more energy than the former, which is consistent with their amplitudes. Clear high EKE distributions are shown in eastern Sri Lanka, especially for cyclonic eddies (Fig. 3j). The high-intensity eddies here are closely related to the southwest monsoon current invading the Bay of Bengal in summer. Generally, due to the southwest monsoon prevailing over the entire North Indian Ocean in summer, the low-latitude equatorial region produces a strong and fast-flowing southwest monsoon current, which enters the Bay of Bengal at a very fast flow rate. Under the influence of the southwest monsoon and the barrier of the Sri Lankan Islands, a significant negative wind stress vorticity occurs in the eastern seas, and a cyclonic eddy often appears here (Dandapat and Chakraborty, 2016). Then, the eddy often interacts with the southwest monsoon current, which makes the eddy rotational speed and eddy intensity significantly stronger (Patnaik et al., 2014). In terms of eddy rotational speed, its maximum value can reach nearly 1 m/s, which is equivalent to the flow velocity of the intrusion current. Therefore, high EKE distributions of cyclonic eddies appear in this area. After that, the cyclonic eddy gradually moves northwest to the western bay, and a compensatory anticyclonic eddy is generated here in autumn (Cui et al., 2016). However, the strength of the anticyclonic eddy is weakened, but its rotational speed is still fast and just slightly lower than that of the cyclone; therefore, there is also a significant EKE distribution of anticyclonic eddies in eastern Sri Lanka. As far as the interior bay, the high EKE is still concentrated in the northwestern bay; that is, eddies accompanying the western boundary current EICC often carry more ocean energy than the eddies in other regions of the bay. At the same time, the mean zonal EKE shows the difference between the cyclonic and anticyclonic eddies in the bay is not significant (Fig. 3l), and the two have obvious EKE difference only in the low-latitude region outside the bay.

4 Three-dimensional thermohaline properties

Before analyzing the three-dimensional thermohaline properties of eddies in the Bay of Bengal, it is necessary to describe of the main water masses in this area. The stratification of water masses plays a vital role in the abnormal temperature and salinity structures caused by eddies. We divided the Bay of Bengal from south to north (0°–20°N) into 10 subregions at intervals of 2° and calculated the average potential temperature and salinity profiles based on all Argo θ/S data in each subregion (Fig. 4). At the surface of the ocean, changes in the water masses of the Bay of Bengal can be clearly seen from south to north. In the low-latitude equatorial area (south of 6°N) outside the bay, the Arabian Sea High-Salinity Water (ASHSW), has a general temperature of

24–30°C and salinity of 34.5–36 and flows to the equator and the Bay of Bengal with seasonal circulation (Emery and Meincke, 1986). In the bay (north of 6°N), the surface salinity decreases from south to north, which represents the surface Bay of Bengal Water (BBW). BBW with a temperature of 25–29°C and salinity of less than 34 presents an obvious surface low-salt property and is mainly formed by abundant precipitation, abundant river injection, and weaker sea surface evaporation in the bay (Emery and Meincke, 1986; Sardessai et al., 2010). Below the surface, water masses present distinct characteristics of Indian Equatorial Water (IEW), with a temperature ranging from 8–23°C and salinity from 34.5–35 (Stramma et al., 1996). It is formed by slowly mixing the ASHSW and deep water and some Indian Central Water (ICW). The mean temperature and salinity profile in the bay (black dotted line in Fig. 4) shows obvious BBW low salinity features on the surface layer and IEW features below the surface layer. To focus on the area within the Bay of Bengal and to exclude the influence of the average climate state of Argo data in low-latitude regions outside the bay, the composition of the three-dimensional eddy structure is limited to the region of 4°–20°N, 80°–94°E.

4.1 *Temperature structures*

Mean potential temperature anomaly θ' diagrams of the composite eddies in the Bay of Bengal are shown in Fig. 5a. Mean θ' caused by eddies can reach 2°C in the thermocline, which is much larger than the Argo-CARS discrepancy quantified by the mean profiles outside eddies (green curve). Compared to the CARS climatology data, the mean profiles outside eddies show vertically averaged temperature biases of 0.14°C. The Argo-CARS systematical bias can reach 0.4°C in the top 100×10^4 Pa. Due to the spatial smoothing, the warm tropical water transported by Indian Ocean circulation is under reflected in the CARS climatology. Therefore, the Argo-CARS systematical bias should to be removed from the mean θ' diagrams. Mean θ' is negative/positive to the cyclonic/anticyclonic eddies in the upper 300×10^4 Pa (Fig. 5a), and below this depth, θ' becomes weak (less than ±0.3°C). In the upper thermocline, negative θ' for cyclonic eddies indicates that the cyclones cool the upper ocean and make a shallow thermocline due to divergence and upwelling. In contrast, anticyclonic eddies with positive θ' tend to warm the subsurface and suppress the thermocline due to convergence and downwelling. The maximum θ' of cyclonic eddies is nearly –2°C at approximately 100×10^4 Pa depth, while the anticyclonic eddies show a maximum θ' of nearly 2°C at 120×10^4 Pa. The results are similar to Gonaduwage et al. (2019) and Gulakaram et al. (2020), but larger than results of Lin et al. (2019). In Lin et al. (2019), they selected Argo profiles within a range of twice eddy radius used to reconstruct the three-dimensional thermohaline structures, so eddy temperature signals may be obscured by Argo profiles that are too far away from the eddy core (Fig. 5 in Lin et al. (2019)). The mean θ' patterns of both eddies exhibit single core vertical structures, and the core of the eddies is located at a depth of approximately 100×10^4–120×10^4 Pa. This outcome occurs mainly because the BBW shows a monotonic and rapid decrease from surface to bottom in the main thermocline (50×10^4–200×10^4 Pa), and there is no double thermocline structure similar to the North Pacific (Yang et al., 2013).

Mean θ' vertical sections of the composite cyclonic and anticyclonic eddies are shown in Figs 5b and c. It can be clearly seen that θ' gradually decreases from the eddy center to the eddy boundary and still reaches a significant signal at the boundary (Δx =±1), even at a distance of 1.5 times the radius (e.g., ±0.5°C in the thermocline layer at Δx =±1.5). This outcome shows that the range of the temperature change caused by eddies is wider than the eddy boundary we identified; however, this spatial range may have exceeded the range of water captured by eddies. In addition, in very shallow surface layers (upper 30×10^4 Pa), the temperature change caused by eddies is not obvious, and θ' is basically less than ±0.1°C. Especially at the sea surface, the temperature anomaly signal is relatively disordered and does not show the same temperature change consistent with the eddy polarity. This outcome may be related to the influence of inflows from the northern Indian Ocean, abundant precipitation and river injection on surface waters in the Bay of Bengal.

Compared with the three-dimensional structure of eddies in other regions, the influence depth of eddies in the Bay of Bengal is relatively shallow and is limited in the upper 300×10^4 Pa. Like some western boundary current regions and the Mediterranean region, the eddy influence depth can reach more than $1\,000\times10^4$ Pa (Chaigneau et al., 2011; Zhang et al., 2016; Hu et al., 2017; Yang et al., 2013). The reason for the shallow influence depth of eddies in the Bay of Bengal is that there are fewer high-intensity eddies that often occur in regions such as the western boundary currents or other strong currents (some eddies with 1 m amplitude occur in the Kuroshio and Gulf Stream regions). The effect of weaker eddies on water cannot reach deep into the ocean. Second, the stratification of the surface waters in the Bay of Bengal is very obvious, which makes the ocean in the bay in a stable stratified state. Especially in summer, because the precipitation greatly exceeds the evaporation and abundant freshwater injection, the surface stratification in the whole northern bay is very obvious, forming a barrier layer at the sea surface, which makes it difficult for eddies to affect the deep ocean.

4.2 *Salinity structures*

The salinity structures inside eddies and outside eddies are given in Fig. 5d. The Argo-CARS salinity bias (green curve) is negative in the upper 100×10^4 Pa of the ocean and is removed from the mean salinity anomaly S' diagrams. The mean salinity anomaly S' inside the cyclonic and anticyclonic eddies from the Argo data also reflect the downwelling/upwelling signal in the Bay of Bengal. The anticyclonic eddies tend to induce a maximum negative salinity anomaly (nearly –0.25) at the subsurface during downwelling due to the sinking of less saline water, while cyclonic eddies prefer to induce a maximum positive salinity anomaly (0.2) due to the advection of more saline water to the surface by upwelling. Generally, a negative perturbation of the salinity anomaly at the surface is observed for the cyclonic eddies, and S' becomes positive below 30×10^4 Pa depth. The mean S' vertical sections of the composite cyclonic and anticyclonic eddies are shown in Figs 5e and f. It can be seen that the surface shallower than 30×10^4 Pa of the cyclonic eddy is covered with negative low-salinity water, and the subsurface of 50×10^4–100×10^4 Pa presents an obvious positive salinity anomaly. For the anticyclonic eddy, there are some messy positive S' signals in the very shallow surface; however, below this, there is a very obvious negative S'. Generally, the effect of eddies on salinity in the Bay of Bengal is concentrated in the upper ocean shallower than 200×10^4 Pa, and the disturbed S' signals in the very shallow surface are related to the influence of inflows from the north Indian Ocean and river injections. Similarly, Lin et al. (2019) and Gulakaram et al. (2020) also showed that the spatial structure of eddy-induced salinity perturbations is characterized by a dominant dipole structure in

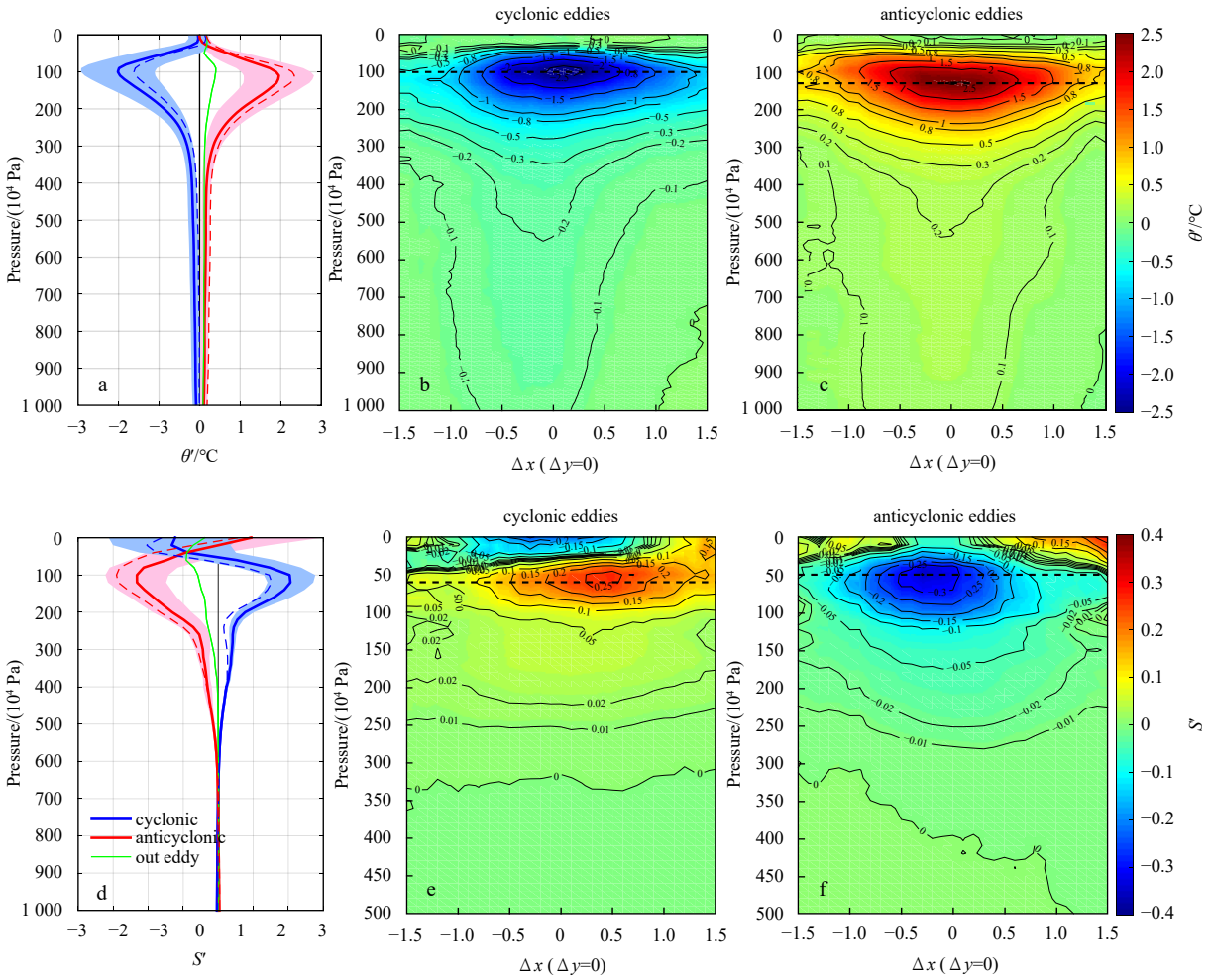

Fig. 5. Mean vertical diagrams of potential temperature anomaly θ' (a) and salinity anomaly S' (d) from Argo profiles as a function of depth inside eddies and outside eddies, mean vertical sections of the potential temperature anomaly θ' (b and c), and salinity anomaly S' (e and f) of the composite cyclonic and anticyclonic eddies at section Δy=0 in the Bay of Bengal (4°–20°N, 80°–94°E), the dashed line indicates the depth of the max θ' and S'. In a and d, the dashed curves indicate the value of the Argo profiles inside eddies minus the CARS climatology, and the green solid curves indicate the mean anomalies that were computed from Argo profiles outside eddies relative to the CARS climatology; the blue and red solid curves correspond to dashed curves that removed the mean anomaly (green solid curves); the shading indicates one standard deviation value range.

the near surface layer. But, in Gonaduwage et al. (2019), the salinity perturbations in surface are not obvious based on all Argo profiles.

Note the salinity structures of positive S' inside cyclonic eddies and negative S' inside anticyclonic eddies in the Bay of Bengal, which are not consistent with other regions. In the northwestern subtropical Pacific Ocean (Yang et al., 2013), the Kuroshio extension region (Dong et al., 2017) and the south Indian Ocean (Hu et al., 2017), cyclonic/anticyclonic eddies predominantly have subsurface (near-surface) intensified negative/positive salinity anomalies. However, the uplifting effect of cyclonic eddies due to divergence and the sinking effect of anticyclonic eddies due to convergence in the Bay of Bengal are obvious. Due to the special characteristics of the water mass in the bay, especially under the control of the low-salinity BBW at the surface and the IEW in the deep ocean, the salinity of seawater shows a monotonic increase with depth. The Bay of Bengal does not have high-salt water masses such as the North Pacific Tropical Water (NPTW) at the subsurface or low-salt water masses such as the North Pacific Intermediate Water (NPIW) in the deep ocean. Therefore, salinity changes caused by eddies in the Bay of Bengal are mainly concentrated in the upper layer and the thermocline, and the salinity changes are relatively monotonic with depth.

4.3 *Regional variety of temperature and salinity structures*

To observe the eddy temperature and salinity structures of cyclones and anticyclones at different longitudes in the Bay of Bengal, we divided the bay from east to west into 14 subregions at 1° longitude intervals and calculated the mean temperature anomaly θ' and salinity anomaly S' profiles in each subregion. In this way, the three-dimensional temperature and salinity structures during the eddy evolution from east to west can be analyzed. The temperature and salinity structures of eddies at different longitudes are shown in longitude-pressure plots of θ' and S', respectively (Fig. 6). It is noted that θ' and S' outside eddies at different longitudes show obvious differences (Figs 6c and f), which indicates Argo-CARS systematical biases at different longitudes. Therefore, when analyzing θ' and S' in eddies at different longitudes, the Argo-CARS biases in this area need to be removed.

Clear images of the gradual eddy structure evolutions are

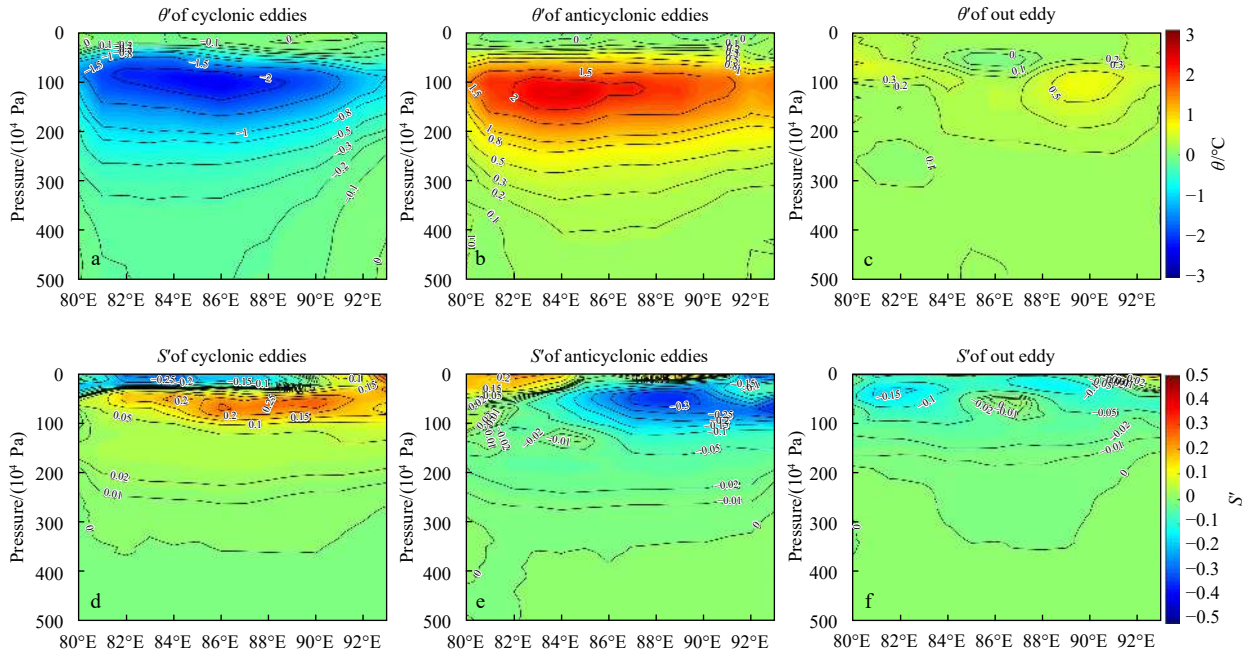

Fig. 6. The potential temperature anomaly θ' (upper panels) and the salinity anomaly S' (bottom panels) of cyclonic (a and d), anticyclonic (b and e) eddies and outside eddies (c and f) at different longitudes. θ' and S' in the eddy removed the Argo-CARS system deviation of its corresponding longitude.

shown in longitude-pressure plots of θ' (Figs 6a and b). The most striking feature is the westward strengthening of eddy signals in both θ' magnitude and effecting depth. For cyclonic or anticyclonic eddies, max θ' values in the eastern bay are approximately –1°C or 1°C at 100×10^4 Pa, but near the western boundary (longitudes less than 86°) the max θ' values can reach –2°C or 2°C at approximately 100×10^4 Pa. As the eddies move westward, θ' induced by the eddies increases, and the effecting depth of the eddies deepens. The strengthening is most prominent at 50×10^4–200×10^4 Pa. In other words, the water at the same temperature in the cyclone/anticyclone is shallower/deeper in the western bay than in the eastern bay, which implies that the uplift (sinking) of eddies in the western bay is more obvious. At the same time, it also shows that the eddy intensity is constantly increasing during the westward propagation, which is consistent with the statistical results of eddy kinetic properties in Section 3.3.

Salinity structures S' of cyclonic and anticyclonic eddies at different longitudes present more complex changes, which are shown in Figs 6d and e. Comparing with S' outside eddies (Fig. 6f), the cyclonic eddies generally induce negative anomalies at the surface in the western and central bay and positive anomalies at the subsurface in the whole bay, while the anticyclonic eddies induce positive anomalies at the surface in the western bay and negative anomalies in central and eastern bay. As the eddies move westward, the salinity structures are more affected by inflows from the North Indian Ocean that result in weakened salinity signals at the subsurface and even opposite signals at the surface in the western bay. The S' of eddies in the upper 50×10^4 Pa is more relevant to the characteristics of the local water mass. The maximum positive S' of the cyclone on the easternmost side of the bay (approximately 93°E) appears on the sea surface, which can even exceed 0.3. Here, low-salinity surface water is formed, which is related to the inflow of freshwater from rivers into the northeast of the bay, such as the Ganges, Bromaputra, and Irrawaddy. Moreover, the salinity S of the surface water gradually decreases from west to east, and the S gradient with pressure becomes larger. Therefore, cyclonic eddies carrying salty water from the subsurface to the surface will cause significant positive salinity anomalies in eastern bay. From the east to the west of the bay, the S' of cyclonic eddies at the surface gradually decreases from positive anomalies to negative anomalies and shows a negative extremum in the western bay. This negative surface S' in the western region may be related to the inflow of high-salinity ASHSW from the North Indian Ocean into the Bay of Bengal during the southwest monsoon in summer and autumn. Especially with the flow of EICC, the high-salinity surface water can basically fill the entire western bay. That is, the west side of the bay is covered with a thin layer of high saline water over the original water mass at a very shallow surface. The cyclonic eddy brings the original low saline water back into the surface due to its lifting effect, so the water mass in the cyclone produces significant negative salinity anomalies. The S' structure of anticyclonic eddies in the western bay also shows the corresponding distribution characteristics. The anticyclonic eddy causes downwelling and the sinking of high saline water at the surface due to convergence, which results in positive salinity anomalies appearing in the upper 50×10^4 Pa in the western bay.

Similarly, the temperature and salinity structures of eddies at different latitudes are shown in Fig. 7. In the north-south direction, the effecting depth of eddies on temperature gradually becomes shallower from north to south (Figs 7a and b). The temperature anomaly θ' in the northern bay is basically at a depth of 50×10^4–200×10^4 Pa and gradually becomes shallower to a depth of 50×10^4–150×10^4 Pa south of 12°N due to the shallower thermocline in the southern bay. At the same time, it was noted that the θ' extrema of cyclonic and anticyclonic eddies are basically concentrated in the areas north of 14°N and south of 10°N, while θ' in the central region of 10°–14°N are generally small. The meridional distribution of this eddy-induced temperature anomaly is not

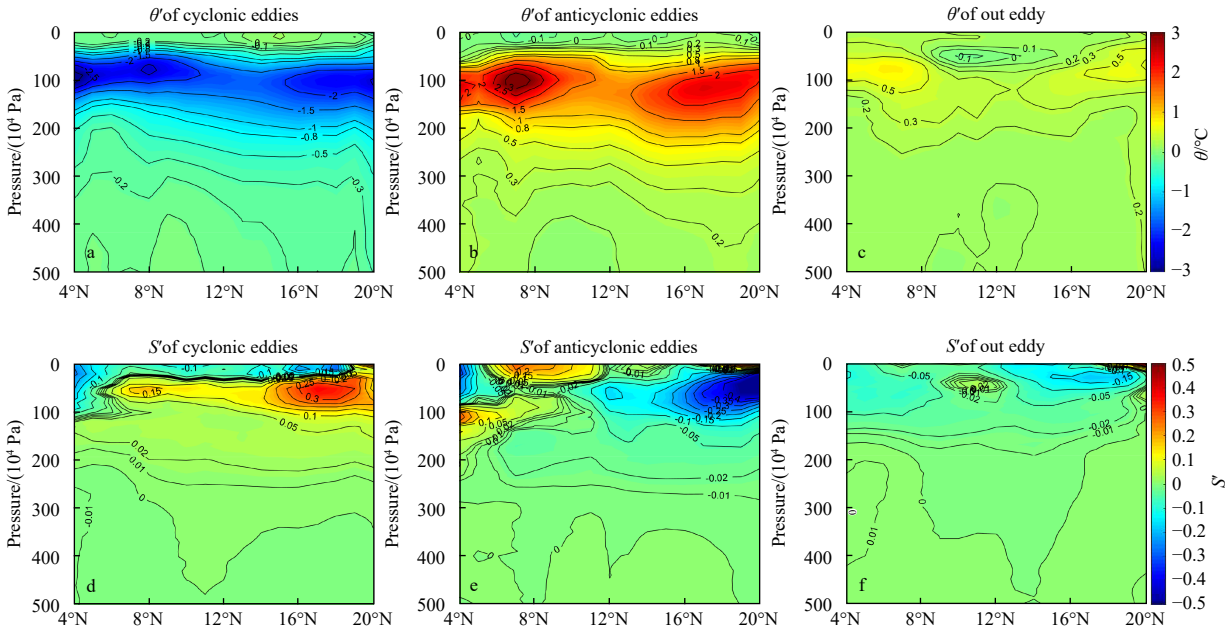

Fig. 7. The potential temperature anomaly θ' (upper panels) and the salinity anomaly S' (bottom panels) of cyclonic (a and d), anticyclonic (b and e) eddies and outside eddies (c and f) at different longitudes. θ' and S' in the eddy removed the Argo-CARS systemdeviation of its corresponding latitudes.

only related to the properties of the water mass, but also related to the eddy intensity of the Bay of Bengal. In the northwestern bay at approximately 14°N, where the EICC occurs seasonally, some high-intensity eddies are more likely to be generated due to the instability of the EICC (see Section 3.3). These high-intensity eddies have more obvious effects on the temperature of the internal water inside eddies, so they can cause large temperature anomalies in the northern bay. The θ' extrema at the latitudes of approximately 8°N are related to the large amplitude and high EKE eddies that often occur during the southwest monsoon in the eastern part of Sri Lanka.

For eddy salinity structures S' at different latitudes (Figs 7c and d), it can be seen that the cyclonic eddies in the northern bay have significant positive S' at the subsurface, and the maximum value can reach 0.35, while the anticyclonic eddies in the northern bay have significant negative S' at the subsurface, and the extremum can reach –0.5. Certainly, this is related to the strong eddies that often occur there. More importantly, the water masses at the surface present obvious characteristics of low saline water due to the inflow of freshwater from rivers into the northeast of the bay. The uplift or sinking of the surface water masses caused by eddies will cause obvious changes in the salinity of the subsurface water masses there. Therefore, once an eddy occurs, it will have obvious salinity anomaly structures. Generally, the halocline of the Bay of Bengal gradually weakens from north to south (Fig. 4), which also causes the value of S' in the halocline to decrease from north to south. Positive S' signals of cyclonic eddies at the subsurface can reach the southernmost side of the bay (approximately 6°N), while negative S' signals of anticyclonic eddies can only reach approximately 10°N. Eddy S' signals at the surface (upper 30×10^4 Pa) show opposite values to the halocline. In terms of cyclonic eddies, the entire surface of the bay presents negative salinity anomalies, especially for the water masses outside the bay (south of 6°N). This is related to the invasion of high-salinity ASHSW from the north Indian Ocean, resulting in a thin layer of high saline water covering the surface in the southern bay, and it will enter the bay with the northward EICC. This phenomenon is more obvious for S' signals of anticyclonic eddies at the surface. The surface upper 50×10^4 Pa in the regions of 6°–10°N corresponds to a significant positive S', which indicates that anticyclonic eddies cause the high-salinity ASHSW to sink below the surface due to convergence.

5 Conclusions

This study analyzes the statistical characteristics and three-dimensional thermohaline properties of mesoscale eddies with a lifetime that exceeds 30 d in the Bay of Bengal. The AVISO altimeter data from January 1993 to February 2017 are used to identify mesoscale eddies using SLA-based eddy identification, track their trajectories, analyze their propagation directions, and characterize their properties. Then, based on Argo profile data and climatology data, the eddy synthesis method was used to construct the three-dimensional temperature and salt structures of the eddies in this area.

Statistical analysis shows most mesoscale eddies propagate westward, while less eddies propagate eastward and occur mainly in the area near the EICC. There is a clear southward (equatorward) preference for eddies with long lifetimes in the Bay of Bengal, especially for cyclones. Moreover, the eddies in different areas of the Bay of Bengal show different north-southward preferences. In terms of eddies with long lifetimes, at the dividing line of 12°N, the eddies in the southern bay mostly propagate northwestward, while the eddies in the middle and northern bay mostly propagate southwestward. The eddies with different propagation preferences in the northern and southern bay are very important for water transport in the Bay of Bengal. In addition, evolution of eddy kinetic properties with lifetime shows that eddies have the significant three-stage feature: the growth period in the former 1/5 of lifetime, the stable period in the middle 2/5 to 4/5 of lifetime, and the dying period in the last 1/5 of lifetime. The census statistics of eddy kinetic properties show that cyclonic eddies are stronger than anticyclones in terms of eddy amp-

litude, EKE, and maximum rotational speed. Clear high EKE distributions are shown in eastern Sri Lanka, especially for cyclonic eddies, which are closely related to the southwest monsoon current invading the Bay of Bengal in summer. Generally, compared with eddies in the regions of strong western boundary currents (e.g., the Gulf Stream and Kuroshio extensions), the mean eddy amplitude in the Bay of Bengal is lower, with fewer large-amplitude eddies. This outcome occurs mainly because the Bay of Bengal has only a seasonal western boundary current EICC that changes with the monsoon, and its velocity and intensity are not as strong as other western boundary currents in the world's oceans.

An investigation of the three-dimensional thermohaline properties of the eddies shows that the mean temperature anomaly θ' is negative/positive to the cyclonic/anticyclonic eddies in the upper 300×10^4 Pa due to upwelling/downwelling, and below this depth, θ' becomes weak. The mainly reason for the shallow influence depth of eddies in the Bay of Bengal is that the stratification of the surface waters in the bay is very obvious, forming a barrier layer at the sea surface which makes it difficult for eddies to affect the deep ocean. At the sea surface, the temperature anomaly signal is relatively disordered and does not show the same temperature change consistent with the eddy polarity due to the influence of inflows from the northern Indian Ocean, abundant precipitation and river injection on surface waters in the Bay of Bengal. The salinity profiles inside eddies also reflect the signal of vertical motion. The cyclonic eddies prefer to induce a positive salinity anomaly at the subsurface due to the uplift of more saline water by upwelling, while anticyclonic eddies tend to induce a negative salinity anomaly due to the sinking of less saline water by downwelling. A negative perturbation of salinity anomaly at the surface is observed for the cyclonic eddies. The salinity structures of positive S' inside cyclonic eddies and negative S' inside anticyclonic eddies in the Bay of Bengal, which are not consistent with other regions. Due to the special characteristics of the water mass in the bay, especially under the control of the low-salinity BBW at the surface and the IEW in the deep ocean, the salinity of seawater shows a monotonic increase with depth.

The temperature structures of cyclonic and anticyclonic eddies at different longitudes in the Bay of Bengal show the westward strengthening of eddy signals in both θ' magnitude and effecting depth. As the eddies move westward, θ' induced by the eddies increases, and the effecting depth of the eddies deepens. From the east to the west of the bay, the salinity structures are more affected by inflows from the North Indian Ocean that result in weakened salinity signals at the subsurface even opposite signals at the surface in the western bay. This negative surface S' of cyclonic eddies in the western is related to the inflow of high-salinity ASHSW from the north Indian Ocean into the Bay of Bengal during the southwest monsoon in summer and autumn. That is, the west side of the bay is covered with a thin layer of high saline water over the original water mass at a very shallow surface. In the north-south direction, the effecting depth of eddies on temperature gradually becomes shallower from north to south due to shallower thermocline in the southern bay. The θ' extrema of cyclonic and anticyclonic eddies are basically concentrated in the areas north of 14°N and south of 10°N. The meridional distribution of this eddy-induced temperature anomaly is not only related to the properties of the water mass, but also related to the eddy intensity of the Bay of Bengal. In the northern bay, the cyclonic eddies have max positive S' at the subsurface and the anticyclonic eddies have max negative S' at the subsurface. The water masses at the surface present obvious characteristics of low saline water due to the inflow of freshwater from rivers into the northeast of the bay. The uplift or sinking of the surface water masses caused by eddies will cause obvious changes in the salinity of the subsurface water masses there. Eddy S' signals at the surface (upper 30×10^4 Pa) show opposite values to the halocline. In terms of cyclonic eddies, the entire surface of the bay presents negative salinity anomalies. This is related to the invasion of high-salinity ASHSW from the north Indian Ocean, resulting in a thin layer of high saline water covering the surface in the southern bay, and it will enter the bay with the northward EICC. This phenomenon is more obvious for positive S' signals of anticyclonic eddies at the surface.

Acknowledgements

The altimeter products (SEALEVEL_GLO_PHY_L4_REP_OBSERVATION_008_47) used here were distributed by the European Copernicus Marine Environment Monitoring Service (CMEMS, marine.copernicus.eu). The Argo profiles are provided by Coriolis Global Data Acquisition Center (www.coriolis.eu.org).

References

Amores A, Melnichenko O, Maximenko N. 2017. Coherent mesoscale eddies in the North Atlantic subtropical gyre: 3-D structure and transport with application to the salinity maximum. Journal of Geophysical Research: Oceans, 122(1): 23–41, doi: 10.1002/2016JC012256

Babu M T, Kumar P S, Rao D P. 1991. A subsurface cyclonic eddy in the Bay of Bengal. Journal of Marine Research, 49(3): 403–410, doi: 10.1357/002224091784995846

Babu M T, Sarma Y V B, Murty V S N, et al. 2003. On the circulation in the Bay of Bengal during northern spring inter-monsoon (March–April 1987). Deep Sea Research Part II: Topical Studies in Oceanography, 50(5): 855–865, doi: 10.1016/S0967-0645(02)00609-4

Chaigneau A, Gizolme A, Grados C. 2008. Mesoscale eddies off Peru in altimeter records: identification algorithms and eddy spatio-temporal patterns. Progress in Oceanography, 79(2–4): 106–119

Chaigneau A, Le Texier M, Eldin G, et al. 2011. Vertical structure of mesoscale eddies in the eastern South Pacific Ocean: A composite analysis from altimetry and Argo profiling floats. Journal of Geophysical Research: Oceans, 116(C11): C11025, doi: 10.1029/2011JC007134

Chelton D B, Gaube P, Schlax M G, et al. 2011a. The influence of nonlinear mesoscale eddies on near-surface oceanic chlorophyll. Science, 334(6054): 328–332, doi: 10.1126/science.1208897

Chelton D B, Schlax M G, Samelson R M. 2011b. Global observations of nonlinear mesoscale eddies. Progress in Oceanography, 91(2): 167–216, doi: 10.1016/j.pocean.2011.01.002

Chen Gengxin, Han Weiqing, Li Yuanlong, et al. 2017. Strong intraseasonal variability of meridional currents near 5°N in the Eastern Indian Ocean: Characteristics and causes. Journal of Physical Oceanography, 47(5): 979–998, doi: 10.1175/JPO-D-16-0250.1

Chen Gengxin, Li Yuanlong, Xie Qiang, et al. 2018. Origins of eddy kinetic energy in the Bay of Bengal. Journal of Geophysical Research: Oceans, 123(3): 2097–2115, doi: 10.1002/2017JC013455

Chen Gengxin, Wang Dongxiao, Hou Yijun. 2012. The features and interannual variability mechanism of mesoscale eddies in the Bay of Bengal. Continental Shelf Research, 47: 178–185, doi: 10.1016/j.csr.2012.07.011

Cheng Xuhua, McCreary J P, Qiu Bo, et al. 2018. Dynamics of eddy generation in the central Bay of Bengal. Journal of Geophysical Research: Oceans, 123(9): 6861–6875, doi: 10.1029/2018JC014100

Cheng Xuhua, Xie Shangping, McCreary J P, et al. 2013. Intraseasonal variability of sea surface height in the Bay of Bengal. Journal of Geophysical Research: Oceans, 118(2): 816–830, doi: 10.1002/jgrc.20075

Cui Wei, Wang Wei, Ma Yi, et al. 2017. Identification and analysis of mesoscale eddies in the Northwestern Pacific Ocean from 1993–2014 based on altimetry data. Haiyang Xuebao (in

Chinese), 39(2): 16–28, doi: 10.3969/j.issn.0253-4193.2017.02.002
Cui Wei, Wang Wei, Zhang Jie, et al. 2019. Multicore structures and the splitting and merging of eddies in global oceans from satellite altimeter data. Ocean Science, 15(2): 413–430, doi: 10.5194/os-15-413-2019
Cui Wei, Yang Jungang, Ma Yi. 2016. A statistical analysis of mesoscale eddies in the Bay of Bengal from 22-year altimetry data. Acta Oceanologica Sinica, 35(11): 16–27, doi: 10.1007/s13131-016-0945-3
Dandapat S, Chakraborty A. 2016. Mesoscale eddies in the Western Bay of Bengal as observed from satellite altimetry in 1993–2014: statistical characteristics, variability and three-dimensional properties. IEEE Journal of Selected Topics in Applied Earth Observations and Remote Sensing, 9(11): 5044–5054, doi: 10.1109/JSTARS.2016.2585179
Dong Di, Brandt P, Chang Ping, et al. 2017. Mesoscale eddies in the northwestern Pacific Ocean: Three-dimensional eddy structures and heat/salt transports. Journal of Geophysical Research: Oceans, 122(12): 9795–9813, doi: 10.1002/2017JC013303
Dong Changming, McWilliams J C, Liu Yu, et al. 2014. Global heat and salt transports by eddy movement. Nature Communications, 5: 3294, doi: 10.1038/ncomms4294
Eigenheer A, Quadfasel D. 2000. Seasonal variability of the Bay of Bengal circulation inferred from TOPEX/Poseidon altimetry. Journal of Geophysical Research: Oceans, 105(C2): 3243–3252, doi: 10.1029/1999JC900291
Emery W J, Meincke J. 1986. Global water masses: Summary and review. Oceanologica Acta, 9(4): 383–391
Fu L L. 2009. Pattern and velocity of propagation of the global ocean eddy variability. Journal of Geophysical Research: Oceans, 114(C11): C11017, doi: 10.1029/2009JC005349
Gonaduwage L P, Chen Gengxin, McPhaden M J, et al. 2019. Meridional and zonal eddy-induced heat and salt transport in the Bay of Bengal and their seasonal modulation. Journal of Geophysical Research: Oceans, 124(11): 8079–8101, doi: 10.1029/2019JC015124
Gulakaram V S, Vissa N K, Bhaskaran P K. 2020. Characteristics and vertical structure of Oceanic mesoscale eddies in the Bay of Bengal. Dynamics of Atmospheres and Oceans, 89: 101131, doi: 10.1016/j.dynatmoce.2020.101131
Hacker P, Firing E, Hummon J, et al. 1998. Bay of Bengal currents during the northeast monsoon. Geophysical Research Letters, 25(15): 2769–2772, doi: 10.1029/98GL52115
Henson S A, Thomas A C. 2008. A census of oceanic anticyclonic eddies in the Gulf of Alaska. Deep Sea Research Part I: Oceanographic Research Papers, 55(2): 163–176, doi: 10.1016/j.dsr.2007.11.005
Hu Dong, Chen Xi, Mao Kefeng, et al. 2017. Statistical characteristics and composed three dimensional structures of mesoscale eddies in the South Indian Ocean. Haiyang Xuebao (in Chinese), 39(9): 1–14, doi: 10.3969/j.issn.0253-4193.2017.09.001
Kumar B, Chakraborty A. 2011. Movement of seasonal eddies and its relation with cyclonic heat potential and cyclogenesis points in the Bay of Bengal. Natural Hazards, 59(3): 1671–1689, doi: 10.1007/s11069-011-9858-9
Le Traon P Y, Faugère Y, Hernandez F, et al. 2003. Can we merge *GEOSAT follow-on* with TOPEX/Poseidon and ERS-2 for an improved description of the ocean circulation?. Journal of Atmospheric and Oceanic Technology, 20(6): 889–895, doi: 10.1175/1520-0426(2003)020<0889:CWMGFW>2.0.CO;2
Legeckis R. 1987. Satellite observations of a western boundary current in the Bay of Bengal. Journal of Geophysical Research: Oceans, 92(C12): 12974–12978, doi: 10.1029/JC092iC12p12974
Lin Xingyu, Qiu Yun, Sun Dezheng. 2019. Thermohaline structures and heat/freshwater transports of mesoscale eddies in the bay of Bengal observed by Argo and satellite data. Remote Sensing, 11(24): 2989, doi: 10.3390/rs11242989
Liu Yu, Dong Changming, Guan Yuping, et al. 2012. Eddy analysis in the subtropical zonal band of the North Pacific Ocean. Deep Sea Research Part I: Oceanographic Research Papers, 68: 54–67, doi: 10.1016/j.dsr.2012.06.001
Lou Hao, Bracco A, Di Lorenzo E. 2011. The interannual variability of the surface eddy kinetic energy in the Labrador Sea. Progress in Oceanography, 91(3): 295–311, doi: 10.1016/j.pocean.2011.01.006
Nencioli F, Dong Changming, Dickey T, et al. 2010. A vector geometry-based eddy detection algorithm and its application to a high-resolution numerical model product and high-frequency radar surface velocities in the Southern California Bight. Journal of Atmospheric and Oceanic Technology, 27(3): 564–579, doi: 10.1175/2009JTECHO725.1
Nuncio M, Kumar S P. 2012. Life cycle of eddies along the western boundary of the Bay of Bengal and their implications. Journal of Marine Systems, 94: 9–17, doi: 10.1016/j.jmarsys.2011.10.002
Pascual A, Faugère Y, Larnicol G, et al. 2006. Improved description of the ocean mesoscale variability by combining four satellite altimeters. Geophysical Research Letters, 33(2): L02611
Patnaik K V K R K, Maneesha K, Sadhuram Y, et al. 2014. East India Coastal Current induced eddies and their interaction with tropical storms over Bay of Bengal. Journal of Operational Oceanography, 7(1): 58–68, doi: 10.1080/1755876X.2014.11020153
Robinson I S. 2010. Mesoscale ocean features: eddies. In: Robinson I S, ed. Discovering the Ocean from Space. Berlin: Springer, 2010
Sardessai S, Shetye S, Maya M V, et al. 2010. Nutrient characteristics of the water masses and their seasonal variability in the eastern equatorial Indian Ocean. Marine Environmental Research, 70(3–4): 272–282
Sarma Y V B, Rao E P R, Saji P K, et al. 1999. Hydrography and circulation of the Bay of Bengal during withdrawal phase of the southwest monsoon. Oceanologica Acta, 22(5): 453–471, doi: 10.1016/S0399-1784(00)87680-X
Schott F A, McCreary Jr J P. 2001. The monsoon circulation of the Indian Ocean. Progress in Oceanography, 51(1): 1–123, doi: 10.1016/S0079-6611(01)00083-0
Somayajulu Y K, Murty V S N, Sarma Y V B. 2003. Seasonal and interannual variability of surface circulation in the Bay of Bengal from TOPEX/Poseidon altimetry. Deep Sea Research Part II: Topical Studies in Oceanography, 50(5): 867–880, doi: 10.1016/S0967-0645(02)00610-0
Souza J M A C, De Boyer Montégut C, Le Traon P Y. 2011. Comparison between three implementations of automatic identification algorithms for the quantification and characterization of mesoscale eddies in the South Atlantic Ocean. Ocean Science, 7(3): 317–334, doi: 10.5194/os-7-317-2011
Stramma L, Fischer J, Schott F. 1996. The flow field off southwest India at 8N during the southwest monsoon of August 1993. Journal of Marine Research, 54(1): 55–72, doi: 10.1357/002224096321344863
Thompson A F, Heywood K J, Schmidtko S, et al. 2014. Eddy transport as a key component of the Antarctic overturning circulation. Nature Geoscience, 7(12): 879–884, doi: 10.1038/ngeo2289
Traon P Y, Dibarboure G. 2004. An illustration of the contribution of the TOPEX/Poseidon—Jason-1 tandem mission to mesoscale variability studies. Marine Geodesy, 27(1–2): 3–13
Vinayachandran P N, Masumoto Y, Mikawa T, et al. 1999. Intrusion of the southwest monsoon current into the Bay of Bengal. Journal of Geophysical Research: Oceans, 104(C5): 11077–11085, doi: 10.1029/1999JC900035
Xu Chi, Shang Xiaodong, Huang Ruixin. 2011. Estimate of eddy energy generation/dissipation rate in the world ocean from altimetry data. Ocean Dynamics, 61(4): 525–541, doi: 10.1007/s10236-011-0377-8
Yang Guang, Wang Fan, Li Yuanlong, et al. 2013. Mesoscale eddies in the northwestern subtropical pacific ocean: statistical characteristics and three-dimensional structures. Journal of Geophysical Research: Oceans, 118(4): 1906–1925, doi: 10.1002/jgrc.20164
Zhang Zhiwei, Tian Jiwei, Qiu Bo, et al. 2016. Observed 3D structure, generation, and dissipation of oceanic mesoscale eddies in the South China Sea. Scientific Reports, 6: 24349, doi: 10.1038/srep24349
Zhang Zhengguang, Wang Wei, Qiu Bo. 2014. Oceanic mass transport by mesoscale eddies. Science, 345(6194): 322–324, doi: 10.1126/science.1252418